**Biophysical Journal, Volume *121***

## Supplemental information

# Slow oscillations persist in pancreatic beta cells lacking phosphofructokinase M

**Isabella Marinelli, Vishal Parekh, Patrick Fletcher, Benjamin Thompson, Jinhua Ren, Xiaoqing Tang, Thomas L. Saunders, Joon Ha, Arthur Sherman, Richard Bertram, and Leslie S. Satin**

# Slow oscillations persist in pancreatic beta cells lacking phosphofructokinase M

I. Marinelli**, V. S. Parekh**, P. A. Fletcher, B. Thompson, J. Ren, X. Tang, T. L. Saunders, J. Ha, A. Sherman, R. Bertram, L. S. Satin

**Co-first authors

## Supporting Material

### 1. List of TaqMan assay probes

| Gene | TaqMan Probe ID | |
|---|---|---|
| | Mouse | Human |
| PFKM | Mm01309576_m1 | Hs01075411_m1 |
| PFKP | Mm00444792_m1 | Hs00737347_m1 |
| PFKL | Mm00435605_mH | Hs01036347_m1 |
| TBP | Mm01277042_m1 | Hs00427620_m1 |

Table S1. List of TaqMan assay probes for gene expression analysis by RT-qPCR.

## 2. Model equations and parameters

The Integrated Oscillator Model (IOM) used in this paper is built upon previously developed mathematical models [1, 2] and consists of modules. The first module describes the cellular electrical activity and intracellular $Ca^{2+}$ dynamics. The second module describes the components of the metabolic pathway included in our model: glycolysis and mitochondrial metabolism.

***The electrical and calcium module***

The rate of change of the cellular membrane potential, $V_M$ , is expressed by

$$\frac{dV_M}{dt} = \frac{1}{\mathrm{C}}\left[I_{\mathrm{Ca}} + I_{\mathrm{K(Ca)}} + I_{\mathrm{K(ATP)}} + I_{\mathrm{K}}\right], \tag{S1}$$

where C is the membrane capacitance, $I_{\mathrm{Ca}}$ is the $V_M$-dependent $Ca^{2+}$ current, $I_{\mathrm{K(Ca)}}$ is the $Ca^{2+}$-activated $K^+$ current, $I_{\mathrm{K(ATP)}}$ is the ATP-dependent $K^+$ current, and $I_{\mathrm{K}}$ is the delayed-rectifying $K^+$ current:

$$I_{\mathrm{Ca}} = g_{\mathrm{Ca}} m_\infty(V_M)(V_M - V_{\mathrm{Ca}}) \ , \tag{S2}$$

$$I_{\mathrm{K(Ca)}} = g_{\mathrm{K(Ca)}} q_\infty(c)(V_M - V_{\mathrm{K}}) \ , \tag{S3}$$

$$I_{\mathrm{K(ATP)}} = g_{\mathrm{K(ATP)}} o_\infty(\mathrm{ADP}, \mathrm{ATP})(V_M - V_{\mathrm{K}}) \ , \tag{S4}$$

$$I_{\mathrm{K}} = g_{\mathrm{K}} n(V_M - V_{\mathrm{K}}) \ . \tag{S5}$$

The upstroke and downstroke of action potentials are mediated by $I_{\mathrm{Ca}}$ and $I_{\mathrm{K}}$, respectively. The K(Ca) and K(ATP) currents are involved in clustering action potentials into bursts.

The activation functions for $I_{\mathrm{Ca}}$, $I_{\mathrm{K(Ca)}}$, and $I_{\mathrm{K(ATP)}}$ are given by

$$m_\infty(V_M) = \frac{1}{1 + \exp[(\upsilon_m - V_M)/s_m]} \ , \tag{S6}$$

$$q_\infty(Ca) = \frac{Ca^2}{k_d^2 + Ca^2} \ , \tag{S7}$$

$$o_\infty(\mathrm{ADP}, \mathrm{ATP}) = \frac{0.08 + 0.89\left(\frac{\mathrm{MgADP}}{k_{dd}}\right)^2 + 0.16\left(\frac{\mathrm{MgADP}}{k_{dd}}\right)}{\left(1 + \frac{\mathrm{MgADP}}{k_{dd}}\right)^2 \left(1 + \frac{\mathrm{ATP}^{4-}}{k_{tt}} + \frac{\mathrm{ADP}^{3-}}{k_{td}}\right)} \ , \tag{S8}$$

with MgADP = 0.165 ADP, $ATP^{4-}$ = 0.05 ATP, and $ADP^{3-}$ = 0.135 ADP. The parameters of this module are given in Table S2.

The activation variable for the delayed-rectifying $K^+$ current, *n*, is given by

$$\frac{dn}{dt} = \frac{n_\infty(V_M) - n}{\tau_n} \quad , \tag{S9}$$

where

$$n_\infty(V_M) = \frac{1}{1 + \exp[(\upsilon_n - V_M)/s_n]} \quad . \tag{S10}$$

The dynamics of the free $Ca^{2+}$ concentration in the cytosol, $Ca$, in the mitochondria, $Ca_{\mathrm{m}}$, and in endoplasmic reticulum (ER), $Ca_{\mathrm{er}}$, are given by

$$\begin{aligned} \frac{dCa}{dt} &= f_{\mathrm{Ca}}(J_{\mathrm{mem}} - J_{\mathrm{er}} - J_{\mathrm{m}}) \quad , \\ \frac{dCa_{\mathrm{m}}}{dt} &= f_{\mathrm{Ca}}\sigma_{\mathrm{m}}J_{\mathrm{m}} \quad , \\ \frac{dCa_{\mathrm{er}}}{dt} &= f_{\mathrm{Ca}}\sigma_{\mathrm{er}}J_{\mathrm{er}} \quad , \end{aligned} \tag{S11}$$

Here, $f_{\mathrm{Ca}}$ is the fraction of $Ca^{2+}$ ions not bound to buffers, and $J_{\mathrm{mem}}$, $J_{\mathrm{m}}$, and $J_{\mathrm{er}}$ represent the $Ca^{2+}$ flux densities across the plasma membrane, into the mitochondria, and into the ER, respectively:

$$J_{\mathrm{mem}} = -\left[\frac{\alpha}{V_{\mathrm{cyt}}} I_{\mathrm{Ca}} + k_{\mathrm{PMCA}} Ca\right] \quad , \tag{S12}$$

$$J_{er} = k_{\mathrm{SERCA}} Ca - k_{NaCa}(Ca_m - Ca) \quad , \tag{S13}$$

$$J_m = J_{\mathrm{uni}} - J_{NaCa} \quad . \tag{S14}$$

The terms $J_{\mathrm{uni}}$ and $J_{\mathrm{NaCa}}$ represent the flux through the $Ca^{2+}$ pumps and through the $Na^+$/ $Ca^{2+}$ exchanger, respectively:

$$J_{\mathrm{uni}} = (p_{21}\psi_{\mathrm{m}} - p_{22})Ca^2 \quad , \tag{S15}$$

$$J_{\mathrm{NaCa}} = p_{21}(Ca_{\mathrm{m}} - Ca)\exp(p_{24}\psi_{\mathrm{m}}) \quad . \tag{S16}$$

| Parameter | Value | Parameter | Value | Parameter | Value |
|---|---|---|---|---|---|
| C | 5300 fF | $k_d$ | 0.5 μM | $\sigma_{er}$ | 31 |
| $g_{Ca}$ | 1000 pS | $k_{dd}$ | 17 μM | $\alpha$ | $5.18 \times 10^{-18}$ μmol$fA^{-1}$ $ms^{-1}$ |
| $g_{K(Ca)}$ | 150 pS | $k_{tt}$ | 1 μM | $V_{cyt}$ | $1.15 \times 10^{-12}$ l |
| $g_{K(ATP)}$ | 19700 pS | $k_{td}$ | 26 μM | $k_{PMCA}$ | 0.2 $ms^{-1}$ |
| $g_K$ | 2700 pS | $\tau_n$ | 20 ms | $k_{SERCA}$ | 0.4 $ms^{-1}$ |
| $V_{Ca}$ | 25 mV | $v_n$ | -16 mV | $p_{21}$ | 0.013 $\mu M^{-1}$ $ms^{-1}mV^{-1}$ |
| $V_K$ | -75 mV | $s_n$ | 5mV | $p_{22}$ | 1.6 $\mu M^{-1}$ $ms^{-1}$ |
| $v_m$ | -20 mV | $f_{Ca}$ | 0.01 | $p_{23}$ | 0.0015 μM $ms^{-1}$ |
| $s_m$ | 12 mV | $\sigma_m$ | 290 | $p_{24}$ | 0.016 $mV^{-1}$ |

Table S1. Parameter values for the electrical and calcium module.

***The metabolic module***

The cytosolic concentrations of F6P and FBP are described by

$$\frac{d\mathrm{F6P}}{dt} = 0.3(J_{GK} - J_{PFK}),$$
$$\frac{d\mathrm{FBP}}{dt} = J_{PFK} - \frac{1}{2}\frac{J_{PDH}}{\sigma_m}, \quad \text{(S17)}$$

where $J_{GK}$ is the glucose-dependent glucokinase (GK) reaction rate, $J_{PFK}$ is the phosphofructokinase (PFK) reaction rate defined in (1), and $J_{PDH}$ is the pyruvate dehydrogenase (PDH) reaction rate. Since the glucose level is the same in all simulations, $J_{GK}$ does not vary. Flux through PDH is described by

$$J_{PDH} = v_{PDH}\frac{1}{K_{NADH_m,PDH} + \frac{NADH_m}{NAD_m}}J_{GPDH}\ , \quad \text{(S18)}$$

where $v_{\mathrm{PDH}}$ is the maximum PDH reaction rate. The glycerol-3-phosphate dehydrogenase (GPDH) reaction rate, $J_{\mathrm{GPDH}}$, is

$$J_{\mathrm{GPDH}} = \frac{Ca_m}{K_{GPDH} + Ca_m}\sqrt{\mathrm{FBP}} \quad . \tag{S19}$$

The adenosine diphosphate (ADP) dynamics are given by

$$\frac{d\mathrm{ADP}}{dt} = J_{\mathrm{hyd}} - \frac{J_{\mathrm{ANT}}}{\sigma_{\mathrm{m}}} \quad , \tag{S20}$$

where $J_{\mathrm{hyd}}$ reflects ATP hydrolysis and $J_{\mathrm{ANT}}$ is the flux of ATP produced in the mitochondria and transported to the cytosol through the adenine nucleotide translocator (ANT),

$$J_{\mathrm{hyd}} = \left(k_{\mathrm{hyd}}Ca + k_{\mathrm{hyd,bas}}\right)\mathrm{ATP} \quad , \tag{S21}$$

$$J_{\mathrm{ANT}} = p_{19}\frac{\frac{\mathrm{ATP_m}}{\mathrm{ADP_m}}}{\frac{\mathrm{ATP_m}}{\mathrm{ADP_m}} + p_{20}}\exp\left(\frac{\mathrm{F}}{2\mathrm{RT}}\psi_{\mathrm{m}}\right) \quad . \tag{S22}$$

The hydrolysis term has a $Ca^{2+}$-independent term that represents ATP hydrolysis for cell homeostasis, and a $Ca^{2+}$-dependent term that represents hydrolysis by $Ca^{2+}$ pumps present on the plasma and ER membranes.

The model assumes that the total nucleotide concentrations in the cytosol and in the mitochondria ($A_{\mathrm{tot}}$ and $A_{\mathrm{tot,m}}$, respectively) is constant, and that the sum of both cytosolic and mitochondrial nucleotides are conserved:

$$\mathrm{ATP} = \frac{1}{2}\left[A_{\mathrm{tot}} + \sqrt{-4\mathrm{ADP}^2 + (A_{\mathrm{tot}} - \mathrm{ADP})^2} - \mathrm{ADP}\right] \quad , \tag{S23}$$

$$\mathrm{ATP_m} = A_{\mathrm{tot,m}}\text{-}\mathrm{ADP_m} \quad . \tag{S24}$$

There are two terms for NADH production: production due to pyruvate dehydrogenase ($J_{PDH}$), and production due to the combined action of dehydrogenases in the citric acid cycle ($J_{DH}$). The mitochondrial concentration of NADH is then

$$\frac{d\mathrm{NADH_m}}{dt} = J_{\mathrm{PDH}} + J_{\mathrm{DH}} - J_{\mathrm{O}} \quad , \tag{S25}$$

where $J_{\mathrm{PDH}}$ is given by (S18) and $J_{\mathrm{DH}}$ and the oxygen consumption rate ($J_O$) are:

$$J_{\mathrm{DH}} = v_{\mathrm{DH}} \frac{Ca_{\mathrm{m}}}{K_{\mathrm{DH}} + Ca_{\mathrm{m}}} \frac{1}{K_{\mathrm{NADH_m,DH}} + \frac{\mathrm{NADH_m}}{\mathrm{NAD_m}}} \quad , \tag{S26}$$

$$J_{\mathrm{O}} = p_4 \frac{\mathrm{NADH_m}}{p_5 + \mathrm{NADH_m}} \frac{1}{1 + \exp\left(\frac{\psi_{\mathrm{m}} - p_6}{p_7}\right)} \quad . \tag{S27}$$

The model assumes nucleotide conservation:

$$\mathrm{NAD_m} = N_{\mathrm{tot,m}} - \mathrm{NADH_m} \quad , \tag{S28}$$

where $N_{\mathrm{tot,m}}$ is the total concentration in the mitochondria.

The changes in the dynamics of the mitochondrial membrane potential, $\psi_{\mathrm{m}}$, are described by

$$\frac{d\psi_{\mathrm{m}}}{dt} = \frac{1}{\mathrm{C_m}} \left[ J_{\mathrm{Hres}} - J_{\mathrm{Hatp}} - J_{\mathrm{Hleak}} - J_{\mathrm{ANT}} - J_{\mathrm{NaCa}} - 2J_{\mathrm{uni}} \right] \quad . \tag{S29}$$

Here, $\mathrm{C_m}$ is the mitochondrial inner membrane capacitance, $J_{\mathrm{Hres}}$ is the flux through respiration-driven proton pumps, $J_{\mathrm{Hatp}}$ is the proton flux entering the mitochondria through the ATPase, while $J_{\mathrm{Hleak}}$ is the proton flux entering the mitochondria through leakage down the proton gradient:

$$J_{\mathrm{Hres}} = p_8 \frac{\mathrm{NADH_m}}{p_9 + \mathrm{NADH_m}} \frac{1}{1 + \exp\left(\frac{\psi_{\mathrm{m}} - p_{10}}{p_{11}}\right)} \quad , \tag{S30}$$

$$J_{\mathrm{Hatp}} = 3J_{\mathrm{F1F0}} \quad , \tag{S31}$$

$$J_{\mathrm{Hleak}} = p_{17}\psi_{\mathrm{m}} - p_{18} \quad . \tag{S32}$$

The term $J_{\mathrm{F1F0}}$ in (S31) is the rate at which the F1F0 ATP synthase phosphorylates ADP to form ATP:

$$J_{\mathrm{F1F0}} = p_{16} \frac{p_{13}}{p_{13} + \mathrm{ATP_m}} \frac{1}{1 + \exp\left(\frac{p_{14} - \psi_{\mathrm{m}}}{p_{15}}\right)} \quad . \tag{S33}$$

Since mitochondrial ATP production comes at the expense of ADP, the mitochondrial ADP level ($\mathrm{ADP}_m$) is given by

$$\frac{d\mathrm{ADP_m}}{dt} = J_{\mathrm{ANT}} - J_{\mathrm{F1F0}} \quad , \tag{S34}$$

with $J_{\mathrm{ANT}}$ and $J_{\mathrm{F1F0}}$ given in (S22) and (S33), respectively.

Parameter values for the metabolic module are given in Table S3.

| Parameter | Value | Parameter | Value | Parameter | Value |
|---|---|---|---|---|---|
| $J_{\mathrm{GK}}$ | 0.001μM $\mathrm{ms^{-1}}$ | $p_4$ | 0.55 μM $\mathrm{ms^{-1}}$ | $p_{15}$ | 8.5 mV |
| $v_{\mathrm{PDH}}$ | 0.4μM $\mathrm{ms^{-1}}$ | $p_5$ | 250 μM | $p_{16}$ | 4 μM $\mathrm{ms^{-1}}$ |
| $K_{\mathrm{NADH_m,PDH}}$ | 1.3 | $p_6$ | 165 mV | $p_{17}$ | 0.0014 μM $\mathrm{ms^{-1}mV^{-1}}$ |
| $K_{\mathrm{GPDH}}$ | 1.5μM | $p_7$ | 5mV | $p_{18}$ | 0.02 μM $\mathrm{ms^{-1}}$ |
| $k_{\mathrm{hyd}}$ | $1.864 \times 10^{-6}$μM $\mathrm{ms^{-1}}$ | $p_8$ | 7.4 μM $\mathrm{ms^{-1}}$ | $p_{19}$ | 0.6μM $\mathrm{ms^{-1}}$ |
| $k_{\mathrm{hyd,\ bas}}$ | $6.48 \times 10^{-7}$μM $\mathrm{ms^{-1}}$ | $p_9$ | 100 μM | $p_{20}$ | 2 |
| $v_{\mathrm{DH}}$ | 1.1μM $\mathrm{ms^{-1}}$ | $p_{10}$ | 165 mV | $A_{\mathrm{tot}}$ | 3000 μM |
| $K_{\mathrm{NADH_m,DH}}$ | 1.3 | $p_{11}$ | 5 mV | $A_{\mathrm{tot,m}}$ | 15000 μM |
| $K_{\mathrm{DH}}$ | 0.8μM | $p_{13}$ | 10000 μM | $N_{\mathrm{tot,m}}$ | 10000 μM |
| $\frac{\mathrm{F}}{2\mathrm{RT}}$ | 0.037 | $p_{14}$ | 190 mV | $\mathrm{C_m}$ | 180 mV |

Table S3. Parameter for the metabolic module.

## 3. Linear mixed effects modelling

To compare the oscillation properties of islets between different groups of animals, care must be taken to account for the fact that measurements from islets have an inherent non-independence: islets from a given mouse are not independent samples when multiple animals are used in a study. In the case of $Ca^{2+}$ imaging, a batch of islets from an individual animal are assayed in one recording, such that inter-animal variability is not present within recordings from a given animal, but only between recordings from different animals. Similarly, variability due to recording conditions occurs when comparing islets from different recordings, but not within a single recording. Finally, within a single recording we recorded islet responses to multiple glucose levels. Linear mixed effects modelling is a technique designed to explicitly handle precisely this type of hierarchical structure in the data. The response variable of interest is modelled as a function of predictor variables (so-called fixed effects) while accounting for the fact that variance is shared among hierarchical groupings in the data (random effects).

To test whether oscillation properties were different between islets from male and female PFKM-KO and wild-type animals, we fit linear models using the R function `lm`, or mixed models using the R function `lmer` from the `lme4` package. For each of voltage, $Ca^{2+}$, and PKAR data, we fit models for oscillation period and plateau fraction. We included PFKM-KO status, sex, and glucose as fixed effects, except in PKAR models where glucose was always 11.1 mM. Mouse, recording, and islet were specified as random effects for the analysis of $Ca^{2+}$ data. For voltage recordings, in which only one islet is measured per recording, recording was omitted as a random effect. For PKAR, islets were only exposed to a single glucose level, so islet was omitted as a random effect. The model specification and fitting summaries are shown below; all models were fit using `REML=TRUE`. Summary tables were generated using the "`tab_model`" function from the R package `sjPlot`, with `p.val="Satterthwaite"` .

***Voltage recordings***

| | Period (min) | | | Plateau Fraction | | |
|---|---|---|---|---|---|---|
| *Predictors* | *Estimates* | *CI* | *p* | *Estimates* | *CI* | *p* |
| (Intercept) | 2.05 | 0.24 – 3.85 | **0.028** | 0.28 | 0.17 – 0.38 | **0.001** |
| Condition [KO] | -1.12 | -2.28 – 0.05 | 0.067 | -0.02 | -0.11 – 0.06 | 0.582 |
| Sex [male] | 0.71 | -0.80 – 2.21 | 0.361 | 0.13 | 0.03 – 0.23 | **0.046** |
| Glucose [11.1] | 2.52 | 1.26 – 3.79 | **<0.001** | 0.29 | 0.25 – 0.34 | **<0.001** |
| **Random Effects** | | | | | | |
| $\sigma^2$ | 3.0313 | | | 0.0041 | | |
| $\tau_{00}$ | 0.0867 $_{Mouse}$ | | | 0.0035 $_{Islet}$ | | |
| | | | | 0.0020 $_{Mouse}$ | | |
| ICC | 0.0278 | | | 0.5730 | | |
| N | 14 $_{Mouse}$ | | | 14 $_{Mouse}$ | | |
| | | | | 21 $_{Islet}$ | | |
| Observations | 38 | | | 38 | | |
| Marginal $R^2$ / Conditional $R^2$ | 0.338 / 0.357 | | | 0.638 / 0.846 | | |

Table S4. Summary of linear mixed modelling of period and plateau fraction in voltage recordings. Model formulas were: Period ~ Condition + Sex + Glucose + (1|Mouse); Plateau Fraction ~ Condition + Sex + Glucose + (1|Mouse) + (1|Islet). The reference group (intercept) was Female Control at 8mM glucose. Estimates, 95% confidence intervals, and p-value (bold, $p<0.05$) for each predictor of Period (left) and Plateau Fraction (right) are shown. A summary of the random effects are also shown: $\sigma^2$, mean variance of random effects; $\tau_{00}$, random intercept variance (between subject variance) for each random effect; ICC, intraclass correlation coefficient (proportion of variance explained by the grouping structure); N, number of groups per random effect; Observations, total number of recordings of islets in any combination of fixed effects; Marginal $R^2$, $R^2$ value considering only fixed effects; Conditional $R^2$, $R^2$ considering both fixed and random effects.

***Calcium recordings***

| | Period (min) | | | Plateau Fraction | | |
|---|---|---|---|---|---|---|
| *Predictors* | *Estimates* | *CI* | *p* | *Estimates* | *CI* | *p* |
| (Intercept) | 5.28 | 4.66 – 5.90 | **<0.001** | 0.32 | 0.25 – 0.40 | **0.005** |
| Condition [KO] | -0.71 | -1.60 – 0.17 | 0.151 | 0.00 | -0.10 – 0.11 | 0.984 |
| Sex [male] | 0.72 | -0.20 – 1.63 | 0.154 | 0.13 | 0.02 – 0.24 | 0.088 |
| Glucose [11.1] | -2.22 | -2.60 – -1.84 | **<0.001** | 0.21 | 0.20 – 0.23 | **<0.001** |
| **Random Effects** | | | | | | |
| $\sigma^2$ | 0.9826 | | | 0.0021 | | |
| $\tau_{00}$ | 0.1487 $_{\text{Recording}}$ | | | 0.0020 $_{\text{Islet}}$ | | |
| | 0.1152 $_{\text{Mouse}}$ | | | 0.0023 $_{\text{Recording}}$ | | |
| | | | | 0.0021 $_{\text{Mouse}}$ | | |
| ICC | 0.2117 | | | 0.7548 | | |
| N | 6 $_{\text{Mouse}}$ | | | 6 $_{\text{Mouse}}$ | | |
| | 10 $_{\text{Recording}}$ | | | 10 $_{\text{Recording}}$ | | |
| | | | | 111 $_{\text{Islet}}$ | | |
| Observations | 156 | | | 156 | | |
| Marginal $R^2$ / Conditional $R^2$ | 0.491 / 0.599 | | | 0.653 / 0.915 | | |

Table S5. Summary of linear mixed modelling of period and plateau fraction in calcium recordings. Model formulas were: Period ~ Condition + Sex + Glucose + (1|Mouse) + (1|Recording); Plateau Fraction ~ Condition + Sex + Glucose + (1|Mouse) + (1|Recording). The reference group was Female Control at 8mM glucose. The meaning of table entries is as in Table S4.

***PKAR recordings***

| | Period (min) | | | Plateau Fraction | | |
|---|---|---|---|---|---|---|
| *Predictors* | *Estimates* | *CI* | *p* | *Estimates* | *CI* | *p* |
| (Intercept) | 7.90 | 6.48 – 9.32 | **<0.001** | 0.59 | 0.53 – 0.64 | **<0.001** |
| Condition [KO] | -1.44 | -2.90 – 0.02 | 0.053 | -0.02 | -0.07 – 0.03 | 0.397 |
| Sex [male] | 0.63 | -0.84 – 2.09 | 0.403 | -0.06 | -0.11 – -0.01 | **0.029** |
| **Random Effects** | | | | | | |
| $\sigma^2$ | 0.59 | | | | | |
| $\tau_{00}$ | 0.34 $_{\text{Recording}}$ | | | | | |
| | 1.11 $_{\text{Mouse}}$ | | | | | |
| ICC | 0.71 | | | | | |
| N | 23 $_{\text{Recording}}$ | | | | | |
| | 14 $_{\text{Mouse}}$ | | | | | |
| Observations | 51 | | | 51 | | |
| Marginal $R^2$ / Conditional $R^2$ | 0.289 / 0.794 | | | 0.096 / 0.058 | | |

Table S6. Summary of linear mixed modelling of period and plateau fraction in PKAR recordings. Model formulas were: Period ~ Condition + Sex + (1|Mouse) + (1|Recording); Plateau Fraction ~ Condition + Sex. The reference group was Female Control at 11mM glucose. The meaning of table entries is as in Table S4.

## 4. Number of mice, islets, and recordings

| Modality | Sex | Condition | Mice | Islets | Recordings |
|---|---|---|---|---|---|
| $V_M$ | female | ctrl | 2 | 3 | 3 |
| | | KO | 1 | 3 | 3 |
| | male | ctrl | 5 | 7 | 7 |
| | | KO | 6 | 8 | 8 |
| $Ca^{2+}$ | female | ctrl | 2 | 55 | 4 |
| | | KO | 1 | 25 | 2 |
| | male | ctrl | 1 | 10 | 1 |
| | | KO | 2 | 22 | 3 |
| PKAR | female | ctrl | 2 | 5 | 3 |
| | | KO | 5 | 15 | 8 |
| | male | ctrl | 5 | 22 | 8 |
| | | KO | 2 | 10 | 4 |

Table S7: Number of mice, islets, and recordings per sex and PFKM-KO condition included in quantitative analysis of period and plateau fraction.

## 5. Summary of islet-level data (sex)

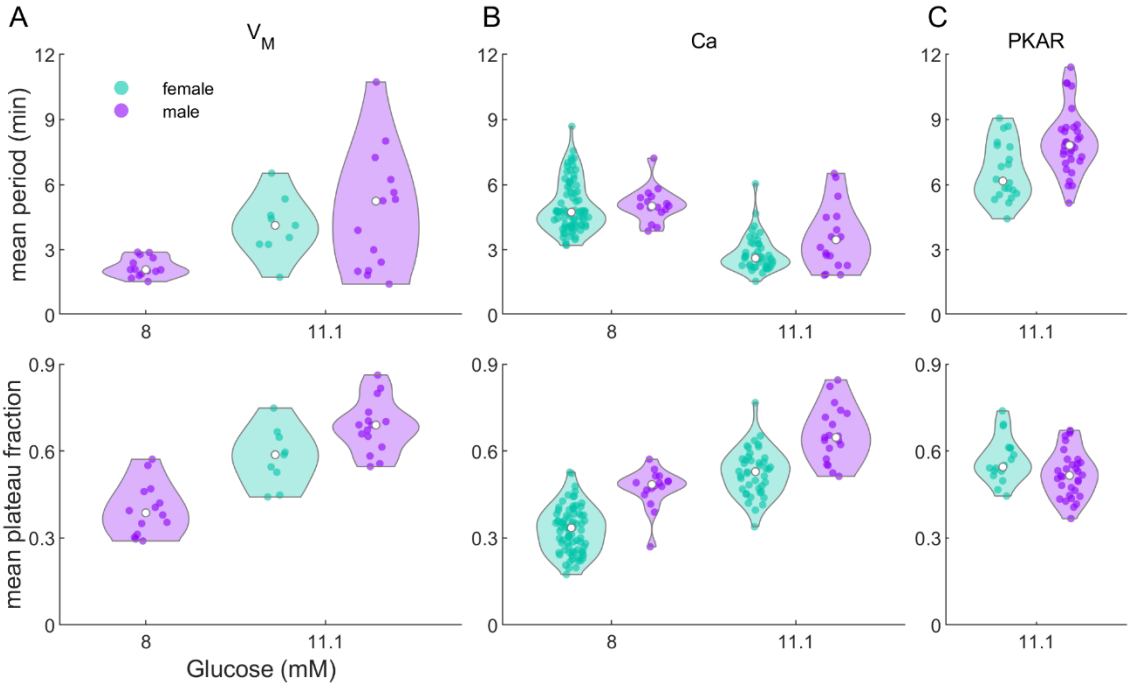


Fig. S1. Comparison of oscillation period and plateau fraction between female and male mice. Violin plots showing mean oscillation period (top panels) and plateau fraction (bottom panels) for islets exposed to specific glucose levels: 8 mM and 11.1mM glucose for membrane potential (panel A) and $Ca^{2+}$ concentration (panel B), or at 11.1 mM glucose for PKAR (panel C). White dots indicate the median across all islets.

# References Cited


1. Bertram, R., et al., *Interaction of glycolysis and mitochondrial respiration in metabolic oscillations of pancreatic islets.* Biophys. J., 2007. **92**(5): p. 1544-55.
2. Marinelli, I., et al., *Transitions between bursting modes in the integrated oscillator model for pancreatic beta-cells.* J. Theor. Biol., 2018. **454**: p. 310-319.